








Received July 11, 2024; accepted November 13, 2024; Date of publication December 02, 2024.  
The review of this paper was arranged by Associate Editor Qobad Shafiee and Editor-in-Chief Heverton A. Pereira.

Digital Object Identifier <http://doi.org/10.18618/REP.e202451>

# Evaluating Adaptive Droop Control for Steady-State Power Balancing in DC Microgrids Using Controller Hardware-in-the-Loop

Beatriz C. Moura <sup>1</sup>, Pedro J. Santos Neto <sup>1</sup>, Danillo B. Rodrigues <sup>2,3</sup>,  
Érico C. Guimarães <sup>2</sup>, Luiz Carlos G. Freitas <sup>2</sup>, João Pedro C. Silveira <sup>4</sup>,  
Gustavo B. Lima <sup>2</sup>

<sup>1</sup>State University of Campinas, Department of Integrated Systems, Campinas, SP, Brazil.

<sup>2</sup>Federal University of Uberlândia, Department of Electrical Engineering, Uberlândia, MG, Brazil.

<sup>3</sup>Federal University of Triângulo Mineiro - Department of Electrical Engineering, Uberaba, MG, Brazil.

<sup>4</sup>State University of Campinas, Electrical and Computer Engineering school, Campinas, SP, Brazil.

e-mail: [mourabeatrizc@gmail.com](mailto:mourabeatrizc@gmail.com); [pedrosn@unicamp.br](mailto:pedrosn@unicamp.br); [danillo.rodrigues@uftm.edu.br](mailto:danillo.rodrigues@uftm.edu.br);  
[erico.guimaraes@ufu.br](mailto:erico.guimaraes@ufu.br); [lcfgfreitas@ufu.br](mailto:lcfgfreitas@ufu.br); [pedro.carvalhosilveira@gmail.com](mailto:pedro.carvalhosilveira@gmail.com); [gustavo.brito.28@ufu.br](mailto:gustavo.brito.28@ufu.br).

**ABSTRACT** DC microgrids (DCMGs) have been gaining attention due to their advantages over AC microgrids. The most commonly used control technique for DCMGs is droop control. Despite its benefits, droop control has drawbacks, such as power mismatch and deviations in DC bus voltage, often caused by differences in line resistance among grid-forming power electronics converters. To address these issues, the article proposes an adaptive droop control technique to correct steady-state power imbalances between grid-forming units in the DCMG. Additionally, a hierarchical voltage level is introduced to regulate the DC bus voltage. The analyzed DCMG includes two energy storage units, electronic loads, and a renewable energy source, each with its respective power electronic converter. The proposed technique uses real-time output power measurements from the energy storage system to calculate line resistance differences, incorporating these into the adaptive droop calculation. Several operating conditions are tested using a controller hardware-in-the-loop. The results validate the proposed technique and design guidelines.

**KEYWORDS** Adaptive droop control, bus voltage regulation, controller hardware-in-the-loop, DC microgrids, power-sharing balance.

## I. INTRODUCTION

Although microgrids are predominantly AC, DC microgrids (DCMG) have become attractive due to their higher efficiency [1]. By using DC, it is possible to eliminate a conversion stage of power electronics converters, resulting in an overall increase in system efficiency. Additionally, DC microgrids offer greater reliability and can be installed in remote areas [2], used to support the conventional grid [3], or in commercial installations [4]. Diverse other advantages of these systems can be explored and detailed in [5].

Various control methods can be applied in DCMGs, all aiming to provide more effective management among the components of the microgrid. One of the most prevalent control techniques is the well-known droop control, characterized as a decentralized system since it does not require communication among the elements of the system, hence, simplicity and robustness can be assured. Despite all the advantages provided by this technique, it incurs some drawbacks such as power mismatch under steady-state conditions [6] and deviation in DC bus voltage [7]. Thus, new variations have been developed to improve power-sharing [8], equalize the state of charge of the energy storage

system [9], improve the robustness of the systems using time-varying models [10], and conduct studies with the aim of hierarchical secondary level layers [11].

In [12], an adaptive droop control is proposed with the aim of improving current sharing and correcting bus voltage deviation. This control system is based on error values between the average output current and average output voltage concerning their respective reference values. Through the secondary control, it regulates the bus voltage and also adjusts the droop constant. However, this control requires different variables, a preliminary calculation to obtain these variables, and an additional controller to adjust the droop coefficient. In the research conducted in [13], an adaptive droop control mechanism is integrated into isolated DC microgrids to optimize power and current sharing. This system employs the least squares technique to estimate real-time feeder resistance values, facilitating the dynamic integration of virtual impedance values in the local control of individual power electronics converters. Nonetheless, the technique uses the estimation of the actual resistances of the feeders. This estimation takes into account three different values for each feeder in the system. Additionally, for the

method proposed in [13], the virtual resistance (or droop constant) of the first feeder is considered to be zero, which is unrealistic.

An adaptive control utilizing the instantaneous average power and the average of droop gains is implemented in [14], in which three additional compensators are employed for voltage-shift control and droop slope adjustment. However, adjusting the droop control in the secondary loop can lead to system failures since the droop control is not performed locally. Furthermore, the control method proposed in [14] requires calculating average values and designing three additional compensators for the control system. The adaptive gain technique, balancing dynamic performance and system stability, presented in [15], utilizes a sliding mode to estimate disturbances within a finite time. The adaptive gain is implemented through a regulation mechanism. The method is more complex as it uses a higher-order sliding mode observer to estimate electrical coupling and an indirect estimation to dynamically adjust the controller parameters, which can also affect the control speed.

Another adaptive droop algorithm, presented in [16], has been developed, in which line resistances are estimated through mathematical calculations. Based on these calculated values, the droop coefficient is adjusted. Additionally, a distributed secondary controller is proposed to enhance load sharing among power electronic converters of different rating levels. As a drawback, this strategy incorporates certain requirements for implementing the control such as designing an additional controller and having knowledge of two other variables to estimate the line resistances. In [17], an adaptive PI droop method is employed as a foundation for adjusting the droop constant values in accordance with the dynamic average of current circulation, aiming to enhance current sharing in the grid-connected mode. Nonetheless, the proposed control requires an additional PI controller to perform the adaptable adjustment of the droop coefficient, which increases complexity.

In [18], an adaptive regulation of input impedance is proposed. In this method, an adaptive virtual impedance is connected in parallel with the input impedance of the load converter, aiming to stabilize the system for different types of source converters. That is, the method is based on knowledge of the frequencies at which the converters operate, requiring a more complex and in-depth analysis for adjusting the input impedance. In the study conducted by [19], the objective was to improve the sharing of load and circulating currents among the converters in the low-voltage DC microgrid (DCMG), so the method calculates the instantaneous virtual resistance based on variations in the converters' output voltages. On the other hand, it is necessary to calculate the droop index and the cable resistance of the converters for determining the droop coefficients, as well as measuring the output voltage. In [20], an adaptive droop control based on virtual output voltage is proposed to reduce voltage deviations and improve power sharing among

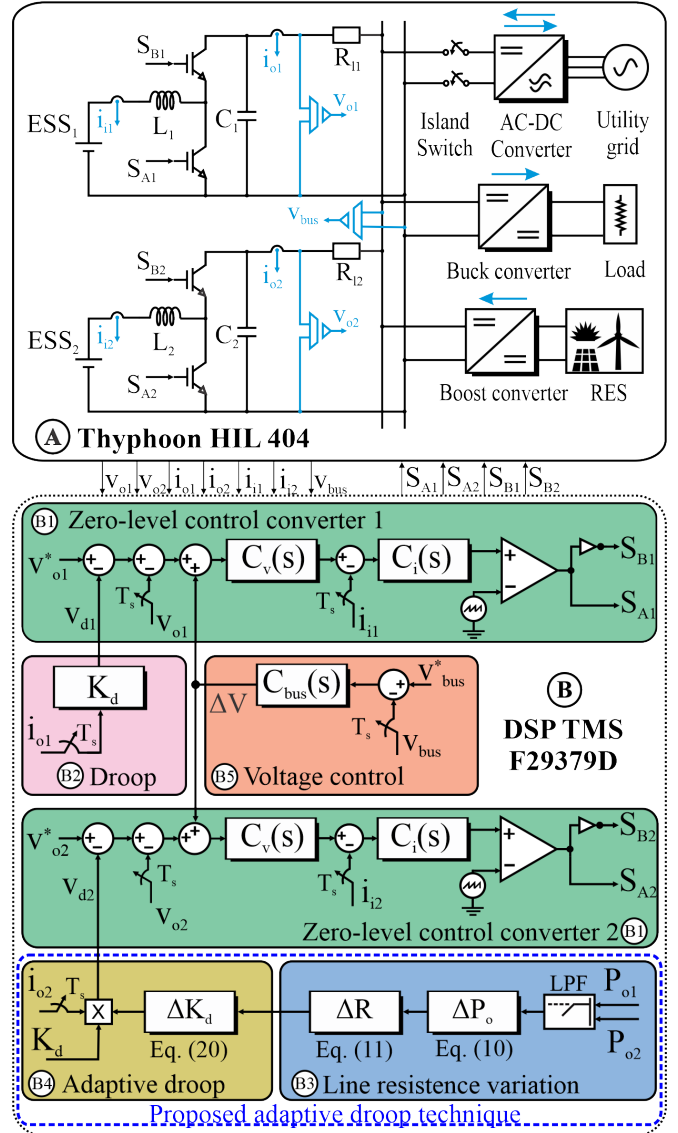


FIGURE 1. The DCMG structure and proposed adaptive droop control implementation.

distributed generations. However, the average value of the units must be known for the adaptable droop adjustment, which is dependent on the point of operation.

Therefore, this article addresses gaps in the field of DC microgrid control by proposing an adaptive droop control technique designed to correct steady-state power imbalances in grid-forming power electronics converters. Existing methods often struggle with dynamic power-sharing and DC bus voltage stabilization, particularly in complex systems with multiple converters. The proposed adaptive droop control technique attempts to fill these gaps by utilizing real-time power calculations to estimate line resistance variations, allowing for more precise and adaptive control without the need for additional, complex controllers. Furthermore, the incorporation of a hierarchical voltage level addresses the challenge of maintaining stable DC bus voltage, a critical

issue in current methodologies. The system's implementation on a Controller Hardware-in-the-Loop (C-HIL) platform, as presented in Fig. 1 with validation across various scenarios, demonstrates the technique's effectiveness and practical applicability, setting the stage for future research to expand and refine this approach.

The advantage of the proposed technique is the real-time monitoring of the line impedance difference based on the variation in output power. By obtaining the value of line resistance variation, it becomes possible to make adjustments to the adaptive droop control. Moreover, the method is simple, requiring minimal information for calculation, and it does not necessitate additional controllers or more sophisticated computations compared to the state-of-the-art methods.

Preliminary results were presented in a conference paper [21] and motivated the authors to conduct further investigations to improve the proposed technique. In the conference paper, simulation results using PSIM software were conducted to evaluate the application of the method. A parametric evaluation was performed to assess the adaptability of this proposal in real systems, considering variations in line resistance disparities. In the presented study, the evaluation and application of the technique are significantly expanded. The line resistance disparities were evaluated at up to twice the initial value. Additionally, this work introduces DC bus voltage correction, which was not addressed in the previous study. Finally, the system is assessed through real-time tests using C-HIL under four new tested scenarios.

The remaining sections of this paper are presented in the following sequence. Section II provides the modeling and description of the DCMG under analysis. Section III presents the conventional droop control and establishes the mathematical foundation for the development of the proposed adaptive droop control methodology. Section IV elaborates the secondary level control. Section V presents the results obtained through C-HIL. Finally, Section VI draws the conclusive remarks.

## II. DCMG DESCRIPTION AND MODELING

### A. DCMG description

A 6 kW rated power DCMG, presented in Fig. 1, is the focal point of this study. The rated power is chosen considering a forthcoming experimental evaluation. The proposed control is structured hierarchically with the overarching goal, as mentioned earlier, of enhancing power sharing between grid-forming converters (DC-DC converters 1 and 2) under steady-state conditions and regulating the DC bus voltage. A DC bus voltage of 400 V has been selected, taking into account applications in data centers, industrial facility standards, electronic equipment design norms, and considerations for improved efficiency [22], [23]. The system parameters used in real-time simulations are outlined in Table 1.

On the top part of the structure, depicted in detail (A) of Fig. 1, one can see that the DCMG is composed of two bidirectional DC-DC converters, which are the grid-forming units for the energy storage system (ESS). Other power electronics converters are used for grid connection, supply electronic loads, and distributed generation (DG) integration. The DG is composed of a renewable energy resource (RES) and a boost converter, which connects the RES to the DC bus. Within this context, it is presupposed that the DG operates at rated power deploying an ordinary boost converter operating with maximum power point tracking technique, such as perturb and observe ( $P\&O$ ). The DC load is fed by an ordinary buck converter and the load adheres to its individual power profile. The AC grid connection is achieved by using an island switch and an ordinary three-phase bidirectional AC-DC converter. The modeling of the components constituting the DCMG is elucidated in the ensuing sections. It is worth mentioning that only the line impedances of the ESS units ( $R_{l1}$  and  $R_{l2}$ ) are displayed in Fig. 1, since they are the object of this study. The line impedances of other units are omitted for simplicity since they have no impact on the proposed control.

On the bottom part of the structure, portrayed in (B) of Fig. 1, one can see the block diagram representing the control strategy embedded in a DSP TMS F28379D from Texas Instruments. In the following tests, the controls were implemented in the same DSP due to limitations with the C-HIL available for testing. The lowest layer of control, designated as zero-level control, is dedicated to the internal regulation of current and voltage loops for each DC-DC converter used to connect the ESS into the DCMG, as shown in (B1) of Fig. 1. The higher layer incorporates the algorithms designed for the determination of the line resistance variation used as an input variable for the proposed adaptive droop control technique, detailed in (B3) and (B4) of Fig. 1. Ultimately, the second level is utilized to reinstate the DC bus voltage to its specified reference set point, as presented in (B5) of Fig. 1. The control strategy is detailed described in the next section.

### B. Bidirectional DC-DC converter modeling

Non-isolated bidirectional converters are employed to connect energy storage systems to the DC bus. The converter is used to perform the charging and discharging of the two ESS present in the DCMG. The differential equations used as a reference for modeling the converter are expressed by (1) and (2) [24], [25].

$$\frac{Ldi_l}{dt} = v_i - v_o(1-d) \quad (1)$$

$$\frac{Cdv_c}{dt} = i_l(1-d) - i_o \quad (2)$$

in which,  $v_i$  and  $v_o$  are the input and output voltage, respectively,  $v_c$  the capacitor voltage,  $i_l$  is the inductor

TABLE 1. System parameters.

Specification	Symbol	Value
<b>Microgrid parameters</b>		
Nominal bus voltage	$V_{bus}$	400 V
Nominal load power	$P_l$	6 kW
Nominal output DG power	$P_{os}$	6 kW
Line resistance 1	$R_{l1}$	1.2 $\Omega$
Line resistance 2	$R_{l2}$	2.4 $\Omega$
DC bus Capacitor	$C_{bus}$	330 $\mu$ F
<b>Bidirectional DC-DC converters 1 and 2</b>		
Inductor	$L$	6.7 mH
Capacitor	$C$	330 $\mu$ F
Rated output current	$I_o$	12.5 A
Rated output power	$P_o$	6 kW
Switching frequency	$f_{sw}$	15 kHz
<b>Control parameters DC-DC converters 1 and 2</b>		
Current controller - proportional gain	$K_{pi}$	0.02901
Current controller - integral gain	$K_{ii}$	33.5
Voltage controller - proportional gain	$K_{pv}$	0.2108
Voltage controller - integral gain	$K_{iv}$	51.8
Bus voltage controller - proportional gain	$K_{pvbus}$	1.5
Bus voltage controller - integral gain	$K_{ivbus}$	37.5
Droop controller gain	$K_d$	2 $\Omega$

current,  $i_o$  is the output current,  $C$  and  $L$  are the capacitor and inductor, and  $d$  is the duty cycle.

### C. Zero-Level control design

The zero-level control consists of an inner current loop and an outer voltage loop, as detailed (B1) of Fig. 1. The controller design is based on the transfer functions associated with the boost operating mode [24], [25], as follows:

$$G_i(s) = \frac{\tilde{i}_l(s)}{\tilde{d}(s)} = \frac{V_o}{Ls} \quad (3)$$

$$G_v(s) = \frac{\tilde{v}_o(s)}{\tilde{i}_l(s)} = \frac{-LI_1s + (1-D)V_o}{V_oCs + 2(1-D)I_1} \quad (4)$$

in which, in steady-state values,  $V_o$  is the output voltage,  $I_l$  inductor current,  $D$  duty cycle,  $L$  is the inductance, and  $C$  is the capacitance.

Equations (3) and (4) are the plants used for designing compensators in each grid-forming unit. For current control, (3) is employed to relate the inductor current with the duty cycle, while (4) relates the converter output voltage to the current passing through the inductor.

The zero-level control is applied to all grid-forming units i.e. for energy storage systems. The current control is typically designed with a crossover frequency one decade below the switching frequency using a conservative phase margin of  $60^\circ$ . For the external voltage control, the crossover frequency is set to a value less than one decade from the crossover frequency of the internal current loop, avoiding interference with its control dynamics and maintaining the same phase margin value as the current control. The equations for these controllers are provided in (5) and (6).

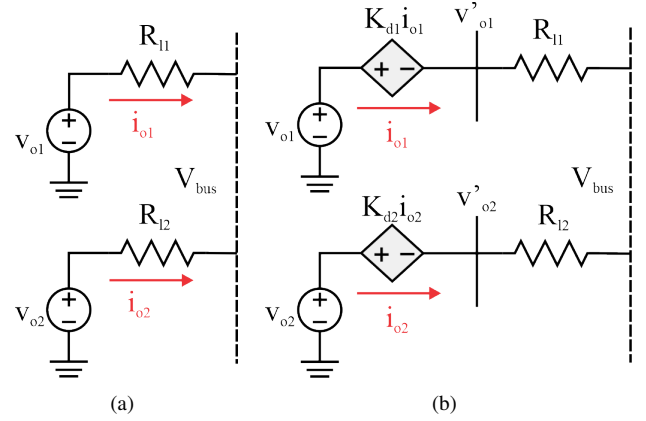


FIGURE 2. DC system simplified model. a) without droop control; b) with droop control.

$$C_i(s) = \frac{K_{pi}s + K_{ii}}{s} \quad (5)$$

$$C_v(s) = \frac{K_{pv}s + K_{iv}}{s} \quad (6)$$

where,  $K_{pi}$  is the proportional gain to current loop,  $K_{pv}$  is proportional gain to voltage loop,  $K_{ii}$  is the integral gain to current loop, and  $K_{iv}$  the integral gain to voltage loop. Table 1 presents the controller values.

## III. PROPOSED ADAPTIVE DROOP CONTROL

### A. Initial droop coefficient calculation

Droop control is depicted in (B2) of Fig. 1. As usual for DC systems, the droop constant  $K_d$  can be calculated by (7) [26].

$$K_d = \frac{\Delta V_o}{\Delta I_o} \quad (7)$$

where  $\Delta V_o$  is the allowed DC bus voltage variation, defined in this work as 12.5% of the 400 V nominal voltage ( $V_{bus}$ ). Thus, the DC bus voltage varies in the range between 375-425 V, following the guidelines established by [27], which indicate that a variation up to  $\pm 15\%$  of the DC voltage does not adversely affect the system components.  $\Delta I_o$  denotes DC-DC converter current taking into account the rated output current. Thus, a constant droop coefficient is defined as equal to 2  $\Omega$ .

### B. Adaptive droop control calculation

In Fig. 1, two bidirectional DC-DC converters operate concurrently, serving as grid-forming units and managing the charging and discharging of the battery banks within an inner control loop. By controlling the output voltage, the simplified system can be represented as a voltage source for each unit, along with the line resistances depicted in Fig. 2(a). The output power for each converter is expressed as

$$\begin{cases} P_{o1} = v_{o1} i_{o1} \\ P_{o2} = v_{o2} i_{o2} \end{cases} \quad (8)$$



Through zero-level control (inner loops), several considerations, given in (9), are possible:

$$\begin{cases} v_{o1} = v_{o2} = v_o \\ R_{l1} = R_l \\ R_{l2} = R_l \cdot \Delta R_l \end{cases} \quad (9)$$

in which,  $v_{o1}$  and  $v_{o2}$  are the output voltage of converter 1 and 2, respectively;  $R_{l1}$  is the line resistances of converter 1,  $R_{l2}$  line resistance of converter 2; and  $\Delta R_l$  is the line resistance variation. The power imbalance ( $\Delta P_o$ ) can be calculated as (10).

$$\Delta P_o = \frac{P_{o1} - P_{o2}}{P_{o1}} = 1 - \frac{1}{\Delta R_l} \quad (10)$$

Hence, since real-time monitoring of the power imbalance is possible, the alteration in line resistance, shown in (B3) of Fig. 1, can be determined by reformulating (10) as (11).

$$\Delta R_l = \frac{1}{1 - \Delta P_o} \quad (11)$$

When the droop control is activated, Fig. 2(b) is considered, where the droop coefficient is included as a dependent voltage source. Therefore, each converter's output power and output voltages are defined as (12).

$$\begin{cases} P_{o1} = v'_{o1} i_{o1} \\ P_{o2} = v'_{o2} i_{o2} \\ v'_{o1} = v_{o1} - K_{d1} i_{o1} \\ v'_{o2} = v_{o2} - K_{d2} i_{o2} \end{cases} \quad (12)$$

Consequently,

$$\Delta P_o = 1 - \beta^2 \alpha \gamma \quad (13)$$

where,

$$\begin{cases} \beta = \frac{R_{l1} + K_{d1}}{R_{l2} + K_{d2}} \\ \alpha = \frac{v_{o2} - V_{bus}}{v_{o1} - V_{bus}} \\ \gamma = \frac{v_{o2} R_{l2} + K_{d2} V_{bus}}{v_{o1} R_{l1} + K_{d1} V_{bus}} \end{cases} \quad (14)$$

in which,  $K_{d1}$  e  $K_{d2}$  are the droop constants, calculated by (7), of converter 1 and 2, respectively; and  $V_{bus}$  is the DC bus voltage.

The zero-level control and the droop control design force the definitions of (9) and (15).

$$\begin{cases} K_{d1} = K_d \\ K_{d2} = K_d \cdot \Delta K_d \end{cases} \quad (15)$$

Therefore, using the considerations in (9) and (15), the power imbalance, given in (13), can be rewritten as (16).

$$\Delta P_o = 1 - \delta^2 \sigma \quad (16)$$

In which,

$$\begin{cases} \delta = \frac{R_l + K_d}{R_l \Delta R_l + K_d \Delta K_d} \\ \sigma = \frac{R_l \Delta R_l v_o + K_d \Delta K_d V_{bus}}{R_l v_o + K_d V_{bus}} \end{cases} \quad (17)$$

If  $V_{bus} = v_o$ , since the voltage variation is limited by the droop control design,  $\Delta P_o$  becomes:

$$\Delta P_o = 1 - \frac{R_l + K_d}{R_l \Delta R_l + K_d \Delta K_d} \quad (18)$$

As a result, the power imbalance in (18) remains unaffected by the measured bus voltage. With real-time measurements of  $\Delta P_o$ , the droop coefficient adjustment  $\Delta K_d$  can be derived based on the steady-state power imbalance, as given in (19).

$$\Delta K_d = \frac{R_l + K_d}{K_d(1 - \Delta P_o)} - \frac{R_l \Delta R_l}{K_d} \quad (19)$$

To address the power discrepancies between the converters,  $\Delta P_o$  is adjusted to zero. As a result, the droop adjustment  $\Delta K_d$  can be expressed by (20).

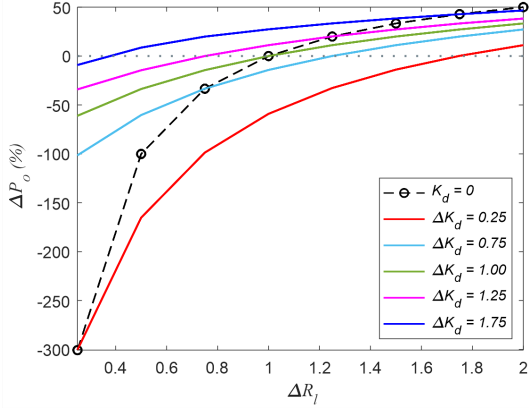
$$\Delta K_d = 1 + \left( \frac{R_l}{K_d} \right) (1 - \Delta R_l) \quad (20)$$

The detailed representation of the proposed adaptive droop control is illustrated in (B4) of Fig. 1. The measured output powers of each converter,  $P_{o1}$  and  $P_{o2}$ , are processed within a low-pass filter to damp power oscillations and achieve stable steady-state value. Moreover, (20) is utilized to calculate the variation in the droop control constant,  $\Delta K_d$ , aiming to eliminate the power imbalance. Subsequently, the output current is multiplied by the droop coefficient, which is dynamically adjusted online through the droop parameter  $\Delta K_d$ .

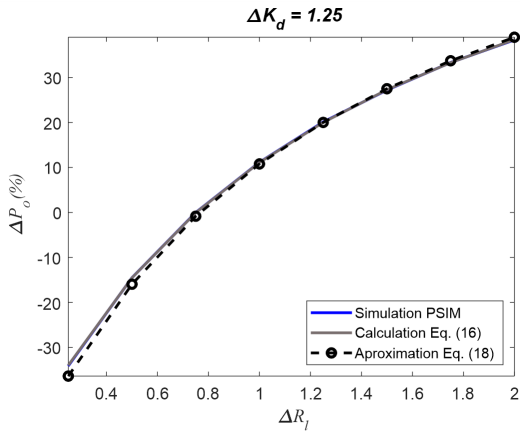
#### IV. PARAMETRIC EVALUATION

In this section, the goal is to investigate the response of the DCMG to parametric variations in droop adjustment,  $\Delta K_d$ , for different line impedance values, as well as the approximation used to obtain the power imbalance,  $\Delta P_o$ , as given in (13). For the parametric evaluations, simulations in PSIM are performed, which includes both converter controllers and the load. In this analysis,  $K_d = 4 \Omega$  (variation of 10% to voltage bus) and  $R_l = 4.275 \Omega$ , assuming real operation on a transmission line of 1 km. Additionally, the values of  $\Delta K_d$  and  $\Delta R_l$  are varied.

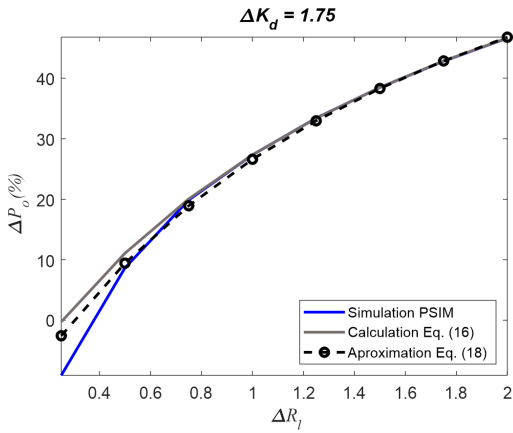
During the variation of the droop coefficient adjustment, the line resistance variation ( $\Delta R_l$ ) is imposed for different  $\Delta K_d$  values. The resulting power variation, given in (10), as a percentage, is illustrated in Fig. 3(a). When  $K_d = 0 \Omega$ , droop control is absent, and only the inner controls of the converters are active. For  $\Delta K_d = 1$ , the droop control is active, and both control systems have equal droop constants ( $K_{d1} = K_{d2} = K_d$ ), where  $K_d$  can be defined as in



(a)



(b)



(c)

FIGURE 3. Parametric evaluation. a)  $\Delta K_d$  adjustment; b) comparison for  $\Delta K_d = 1.25$ ; c) comparison for  $\Delta K_d = 1.75$ .

(7). When  $\Delta K_d < 1$  or  $\Delta K_d > 1$ , the system operates adaptively, as given in (20).

The analyses shown in Fig. 3(b) and Fig. 3(c) compare both forms of calculation of  $\Delta P_o$  and the results from PSIM simulations. The power imbalance is calculated using (16), while its proposed approximation, representing the simplified

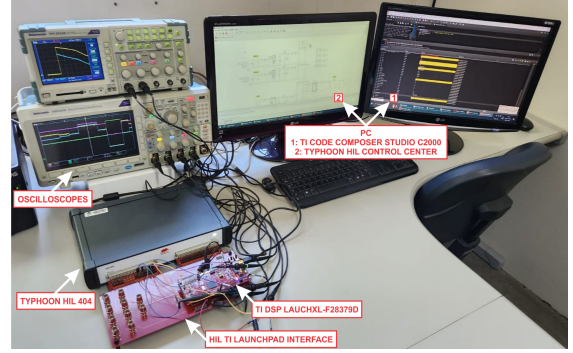


FIGURE 4. C-HIL setup.

expression, is given by (18). In Fig. 3(b), the results for  $\Delta K_d = 1.25$  are shown. It is observed that there is no significant difference between the simulations and the calculated equations. Specifically, for  $\Delta R_l < 0.8$ , the approximated power imbalances calculation deviates less than 10% from the simulation. However, as the droop adjustment increases, e.g.  $\Delta K_d = 1.75$ , Fig. 3(c), differences arise for values of  $\Delta R_l < 1$ .

A detailed parametric analysis of the method can be found in the conference paper [21]. Based on this investigation, one can conclude that the approximations used to derive the droop coefficient adjustment are effective for a wide range of line impedance variations. Nonetheless, significant voltage drops may occur in the DC bus when  $\Delta K_d$  increases, which suggests that the method design should take into account limited line resistance disparities in DCMGs.

## V. DESIGN OF SECONDARY LEVEL CONTROL

The main purpose of the secondary level is to maintain the DC bus voltage within the nominal value of 400 V. This is achieved by an external PI controller outer to the previously designed controls, as illustrated in (B5) of Fig. 1. The considered value of crossover frequency is chosen such that it does not interfere with the previously developed loops. Therefore, the second level is considered a slower loop than the others. The same DSP is used to implement the control of the DCMG due to limitations of the C-HIL available for testing. The controller equation, presented in (21), was designed based on the plant described in (22).

$$C_{v_{bus}}(s) = \frac{K_{pbus}s + K_{ibus}}{s} \quad (21)$$

$$G_{v_{bus}}(s) = \frac{1}{C_{bus}s} \quad (22)$$

in which,  $K_{pbus}$  is the proportional gain,  $K_{ibus}$  is integral gain to secondary loop control, and  $C_{bus}$  is the DC bus capacitance (see Table 1)

## VI. CONTROLLER HARDWARE-IN-THE-LOOP RESULTS

The configuration of the DCMG depicted in (A) of Fig. 1 was replicated using a Typhoon HIL 404 for system modeling.

Simultaneously, the control system was implemented on a TI Digital Signal Processor (DSP) TMS LAUNCHXL-F28379D. Integration of both devices was facilitated through a HIL TI Launchpad interface, constituting the C-HIL platform showcased in Fig. 4. The results were derived from oscilloscopes (with adjusted values) and HIL SCADA. The system's performance was evaluated across four unique scenarios, outlined as follows:

- Test 1: conventional droop control is applied to the DCMG, in which parameters such as power flow, DC-bus voltage, and the state-of-charge (SOC) of the battery banks are examined.
- Test 2: The proposed adaptive droop control is incorporated into the system. The performance evaluation was done using the same parameters as those in Test 1.
- Test 3: During the test, the proposed adaptive droop control is deliberately deactivated, simulating a scenario of communication loss within the DCMG. As a result, the system is compelled to revert to operating under conventional droop control, thus evaluating the control robustness.
- Test 4: The secondary control is applied to the system to regulate the bus voltage. In this case, the control is designed to maintain the nominal voltage at any control level, thus verifying the hierarchical approach.

In the subsequent simulation tests,  $P_{o1}$  and  $P_{o2}$  denote the output power of the ESS bidirectional DC-DC converters, referred to as converters 1 and 2. Similarly,  $P_{os}$  and  $P_l$  represent the power of the distributed generator and load, respectively. The DC-bus voltage is denoted by  $V_{bus}$ . The state-of-charge of each ESS is specified as  $SOC_1$  (starting at 80%) and  $SOC_2$  (starting at 85%), respectively.

In Test 1, droop control is implemented in the system starting from  $t_2$  in Fig. 5. In Fig. 5(a), initially, only converter 1 ( $P_{o1}$ ) supplies the load ( $P_l$ ) at  $t_1$ . Converter 2 ( $P_{o2}$ ) is connected to the bus and both converters begin to share power but in an unbalanced manner, with the units operating in discharge mode. In this case, converter 1 supplies more power to the load than converter 2 due to the inherent line resistance difference in the system, considering a variation  $\Delta R_l = 2$ . When droop control is applied to the system, (in this case,  $K_d = 2 \Omega$  for both grid-forming converters, as previously calculated) there is an improvement in power sharing. However, the power-sharing is still not done equally, reducing the power difference ( $\Delta P_o$ ) from approximately 58%, when only inner loops operate on the DCMG, to 33%, when the droop control is activated. With the load variation, from  $t_3$  to  $t_4$ , the difference in power-sharing still prevails. The distributed generation (DG) supplies the DCMG, starting from  $t_5$ , causing  $P_{o1}$  and  $P_{o2}$  to have a negative value as the units now begin to charge.

The bus voltage, shown in Fig. 5(b), in the zero-level control (from  $t_0$  to  $t_2$ ) always operates close to the 400 V level, experiencing a greater transient at  $t_1$ , when converter

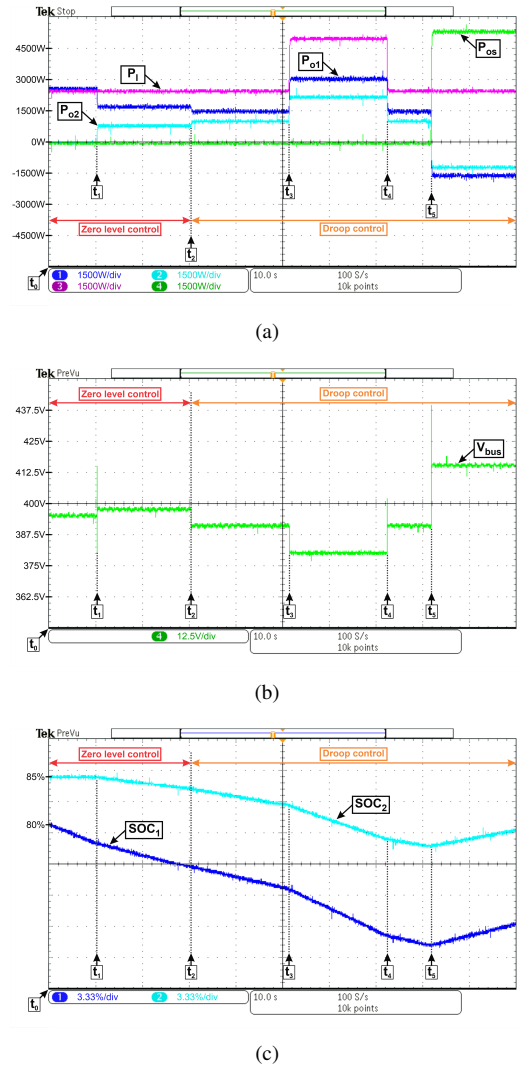
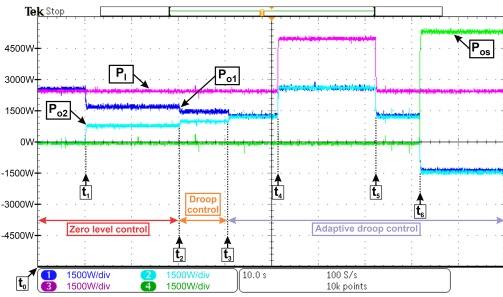


FIGURE 5. Test 1 - Conventional droop control. a) Power flow; b) DC-bus voltage; c) Battery banks state-of-charge.

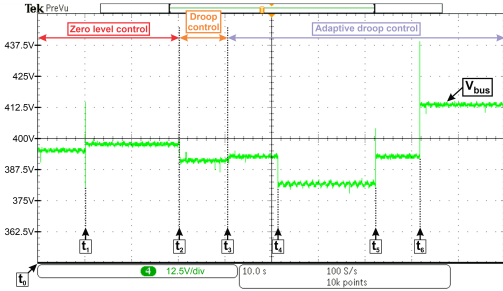
2 is connected to the system. In droop control, the bus voltage operates within the range of 375-425 V, as detailed in subsection III. A. As power increases, the voltage decreases, reaching a minimum value of 380 V when the load power is augmented. A higher-level overshoot is found at  $t_5$  due to the connection of DG to the DCMG. There is also an overshoot incidence at  $t_4$  of approximately 4.4%.

The state-of-charge value of each battery bank is illustrated in Fig. 5(c). As the units act as grid formers, they initially start to discharge, resulting in a slope in the state-of-charge.  $SOC_2$  remains at the initial value until its connection to the system. Therefore, the droop control input only impacts SOC curves in load variations, when DG operates in the system ( $t_3$ ,  $t_4$ , and  $t_5$ ) and when energy storage systems start to charge. In this case, DG supplies the load and charges the ESS.

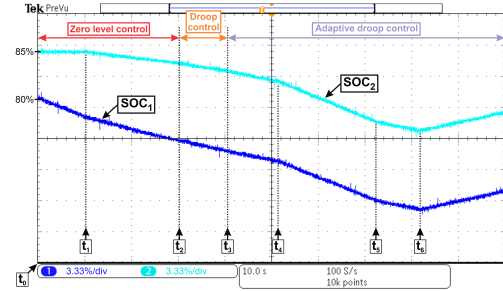
In Test 2, presented in Fig. 6, the proposed adaptive droop control is activated. In this case,  $\Delta K_d$  varies according



(a)



(b)



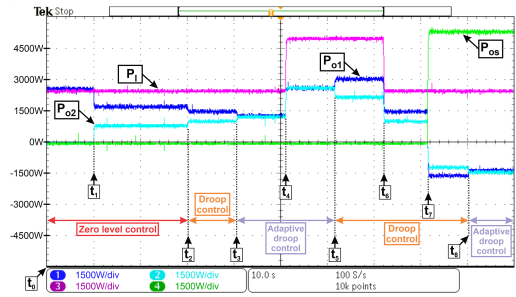
(c)

FIGURE 6. Test 2 - Adaptive droop control. a) Power flow; b) DC-bus voltage; c) Battery banks state-of-charge.

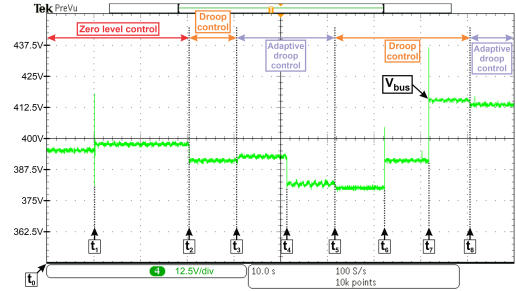
to (20). As this equation depends on the variation in line resistance, it can be calculated online from (11), because the equation depends solely on  $\Delta P_o$ . The proposed control is implemented at  $t_3$ . One can observe from Fig. 6(a) that the ESS power imbalance,  $\Delta P_o$ , is fully mitigated. Even with a load variation, the sharing between units is accurate, as the incompatibility is determined by the variation in line resistance.

Under the proposed control, the bus voltage from  $t_4$  to  $t_5$  is 381.2 V, as illustrated in Fig. 6(b), indicating an increase in voltage with a deviation of 4.7%, instead of 5% shown in Fig. 5(b) (from  $t_3$  to  $t_4$ ). The state-of-charge, presented in Fig. 6(c), exhibit the same behavior as explained in Test 1, but with a smaller variation in the same period. In Fig. 5(c), at  $t_5$ , the variation among the SOC<sub>s</sub> is 15.8%, while at  $t_6$ , in Fig. 6(c), this variation is reduced to 12.7%.

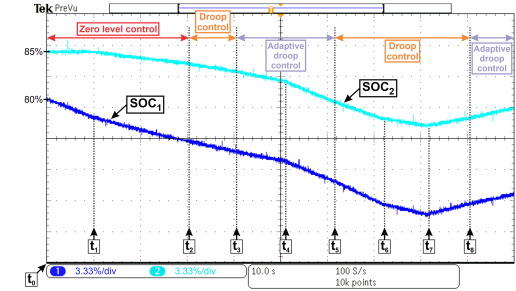
In Test 3, depicted in Fig. 7, a communication failure is introduced into the system from  $t_5$  to  $t_8$ . Even with power



(a)



(b)



(c)

FIGURE 7. Test 3 - Adaptive droop control with lost communication. a) Power flow; b) DC-bus voltage; c) Battery banks state-of-charge.

load variations ( $P_l$ ) and the connection of the DG to the system, the control achieves its objective of power-sharing (unbalanced). During this period, the system operates under conventional droop control. The DC bus voltage during the communication loss period stays within the calculated limits, as shown in Fig. 7(b). Therefore, the robustness of the control can be observed, as it can be recovered. This is due to the fact that once  $\Delta R_l$  is calculated in the inner control, its value is stored, meaning that once the necessary information has been saved, thus the droop adjustment ( $\Delta K_d$ ) can be reused when the communication line is restored.

In Test 4, given in Fig. 8, the system experiences load variations ( $t_4$  to  $t_5$ ) and the connection of the DG at  $t_6$ . The secondary control is implemented starting from  $t_7$ . It is noticeable that precise power sharing is achieved in instants  $t_3$  to  $t_7$  and again from  $t_{10}$  to  $t_{14}$ , in Fig. 8(a). The voltage regulation is illustrated in Fig. 8(b), in which its value is fixed at 400 V with a ripple of less than 1%, staying



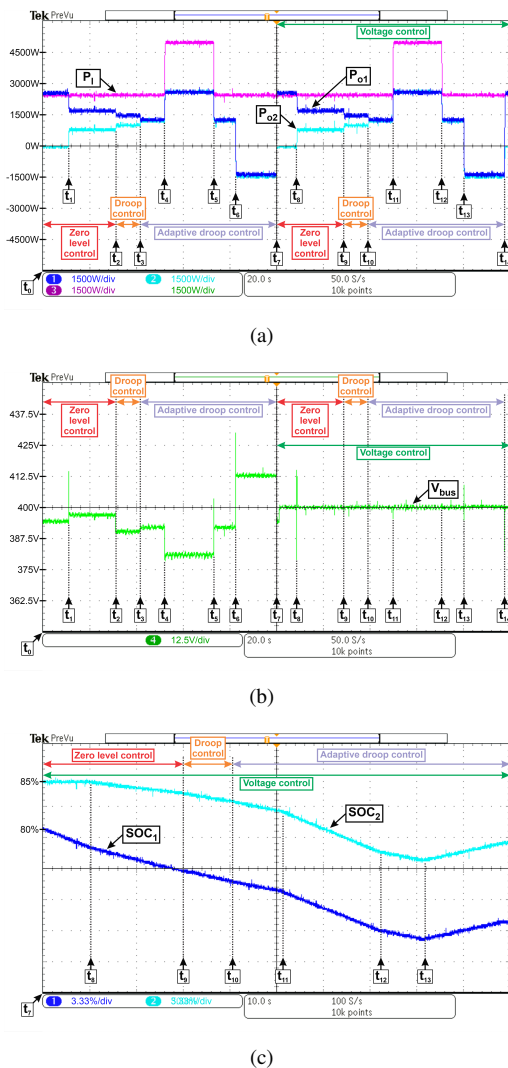


FIGURE 8. Test 4 - DC bus voltage regulation. a) Power flow; b) DC-bus voltage; c) Battery banks state-of-charge.

within acceptable limits. The SOC's values, in Fig. 8(c), are illustrated from  $t_8$  onward since the system's behavior remains the same.

## VII. CONCLUSION

This article presented an adaptive droop control technique that aims to correct the steady-state power imbalances between the grid-forming units of a DCMG. The proposed control utilizes real-time calculated power values to estimate the difference between line resistances, employing this information for adaptive calculations. The proposed method is precise, simple to implement in a digital controller, and robust to communication failure. Additionally, a hierarchical voltage level was implemented to regulate the DC bus voltage. The DCMG was implemented using a Typhoon HIL 404 for system modeling. Simultaneously, the control system was implemented on a TI Digital Signal Processor TMS LAUNCHXL-F28379D. Integration of both devices

was facilitated through a HIL TI Launchpad interface, constituting the C-HIL platform. The system's performance was evaluated across four unique scenarios. The presented results confirm the effectiveness of the proposed adaptive droop control technique. This method also reduces the deviation between the state of charges of energy storage systems. In the future perspectives, there is an intention to conduct a stability analysis to establish the limits of the application of this control and expand the methodology to more grid-forming units to verify extended plug-and-play capability.

## ACKNOWLEDGMENT

This work was financially supported in part by the Universidade Federal de Uberlândia, in part by State University of Campinas, and in part by the following Brazilian research funding agencies: Fundação de Amparo à Pesquisa do Estado de Minas Gerais (Fapemig) Grant APQ-04929-22, Coordenação de Aperfeiçoamento de Pessoal de Nível Superior (CAPES) – Finance Code 001, Grants 88887.001158/2024-00, Conselho Nacional de Desenvolvimento Científico e Tecnológico (CNPq) – Grants 303085/2022-3, 407403/2022-1, 406881/2022-7, 408529/2023-7.

## AUTHOR'S CONTRIBUTIONS

**MOURA, B. C.:** Conceptualization, Data Curation, Formal Analysis, Investigation, Methodology, Software, Validation, Visualization, Writing – Original Draft, Writing – Review & Editing. **SANTOS NETO, P. J.:** Conceptualization, Formal Analysis, Funding Acquisition, Investigation, Methodology, Project Administration, Resources, Software, Supervision, Validation, Visualization, Writing – Review & Editing. **RODRIGUES, D. B.:** Data Curation, Investigation, Software, Validation. **GUIMARÃES, E. C.:** Data Curation, Investigation, Software, Validation. **FREITAS, L. C. G.:** Formal Analysis, Project Administration, Resources, Software, Supervision, Validation, Visualization, Writing – Review & Editing. **SILVEIRA, J. P. C.:** Formal Analysis, Software, Visualization, Writing – Review & Editing. **LIMA, G. B.:** Software, Visualization.

## PLAGIARISM POLICY

This article was submitted to the similarity system provided by Crossref and powered by iThenticate – Similarity Check.

## REFERENCES

- [1] S. Parhizi, H. Lotfi, A. Khodaei, S. Bahramirad, "State of the Art in Research on Microgrids: A Review", *IEEE Access*, vol. 3, pp. 890–925, jun 2015, doi:10.1109/ACCESS.2015.2443119.
- [2] A. Marahatta, Y. Rajbhandari, A. Shrestha, A. Singh, A. Gachhadar, A. Thapa, "Priority-based low voltage DC microgrid system for rural electrification", *Energy Reports*, vol. 7, pp. 43–51, 2021, doi:10.1016/j.egy.2020.11.030.
- [3] P. García-Triviño, J. P. Torreglosa, L. M. Fernández-Ramírez, F. Jurado, "Control and operation of power sources in a medium-voltage direct-current microgrid for an electric vehicle fast charging station with a photovoltaic and a battery energy storage system", *Energy*, vol. 115, pp. 38–48, nov 2016, doi:10.1016/j.energy.2016.08.099.

- [4] B. T. Patterson, "DC, Come Home: DC Microgrids and the Birth of the "Enernet"", *IEEE Power and Energy Magazine*, vol. 10, no. 6, pp. 60–69, nov 2012, doi:10.1109/MPE.2012.2212610.
- [5] Z. Yi, X. Zhao, D. Shi, J. Duan, Y. Xiang, Z. Wang, "Accurate Power Sharing and Synthetic Inertia Control for DC Building Microgrids With Guaranteed Performance", *IEEE Access*, vol. 7, pp. 63698–63708, 2019, doi:10.1109/ACCESS.2019.2915046.
- [6] M. Yuan, Y. Fu, Y. Mi, Z. Li, C. Wang, "Hierarchical control of DC microgrid with dynamical load power sharing", *Applied Energy*, vol. 239, no. November 2018, pp. 1–11, apr 2019, doi:10.1016/j.apenergy.2019.01.081.
- [7] Y. Xia, W. Wei, Y. Peng, P. Yang, M. Yu, "Decentralized Coordination Control for Parallel Bidirectional Power Converters in a Grid-Connected DC Microgrid", *IEEE Transactions on Smart Grid*, vol. 9, no. 6, pp. 6850–6861, nov 2018, doi:10.1109/TSG.2017.2725987.
- [8] M. Mokhtar, M. I. Marei, A. A. El-Sattar, "An Adaptive Droop Control Scheme for DC Microgrids Integrating Sliding Mode Voltage and Current Controlled Boost Converters", *IEEE Transactions on Smart Grid*, vol. 10, no. 2, pp. 1685–1693, mar 2019, doi:10.1109/TSG.2017.2776281.
- [9] J. Su, K. Li, Y. Li, C. Xing, J. Yu, "A Novel State-of-Charge-Based Droop Control for Battery Energy Storage Systems to Support Coordinated Operation of DC Microgrids", *IEEE Journal of Emerging and Selected Topics in Power Electronics*, vol. 11, no. 1, pp. 312–324, feb 2023, doi:10.1109/JESTPE.2022.3149398.
- [10] T. V. Vu, D. Perkins, F. Diaz, D. Gonsoulin, C. S. Edrington, T. El-Mezyani, "Robust adaptive droop control for DC microgrids", *Electric Power Systems Research*, vol. 146, pp. 95–106, may 2017, doi:10.1016/j.epsr.2017.01.021.
- [11] J. C. Neves, R. D. Silveira, S. A. O. Da Silva, L. P. Sampaio, "Estudo e Implementação de Controle Secundário em Microrredes CC", *Eletrônica de Potência*, vol. 29, p. e202416, jun 2024, doi:10.18618/REP.2005.1.053061.
- [12] R. Kumar, M. K. Pathak, "Distributed droop control of dc microgrid for improved voltage regulation and current sharing", *IET Renewable Power Generation*, vol. 14, no. 13, pp. 2499–2506, oct 2020, doi:10.1049/iet-rpg.2019.0983.
- [13] N. Mohammed, L. Callegaro, M. Ciobotaru, J. M. Guerrero, "Accurate power sharing for islanded DC microgrids considering mismatched feeder resistances", *Applied Energy*, vol. 340, no. January, p. 121060, jun 2023, doi:10.1016/j.apenergy.2023.121060.
- [14] S. Liu, H. Miao, J. Li, L. Yang, "Voltage control and power sharing in DC Microgrids based on voltage-shifting and droop slope-adjusting strategy", *Electric Power Systems Research*, vol. 214, no. PA, p. 108814, jan 2023, doi:10.1016/j.epsr.2022.108814.
- [15] X. Wang, X. Dong, X. Niu, C. Zhang, C. Cui, J. Huang, P. Lin, "Toward Balancing Dynamic Performance and System Stability for DC Microgrids: A New Decentralized Adaptive Control Strategy", *IEEE Transactions on Smart Grid*, vol. 13, no. 5, pp. 3439–3451, sep 2022, doi:10.1109/TSG.2022.3167425.
- [16] N. Ghanbari, S. Bhattacharya, "Adaptive Droop Control Method for Suppressing Circulating Currents in DC Microgrids", *IEEE Open Access Journal of Power and Energy*, vol. 7, no. 1, pp. 100–110, 2020, doi:10.1109/OAJPE.2020.2974940.
- [17] A. Nawaz, J. Wu, J. Ye, Y. Dong, C. Long, "Circulating current minimization based adaptive droop control for grid-connected DC microgrid", *Electric Power Systems Research*, vol. 220, no. February, p. 109260, jul 2023, doi:10.1016/j.epsr.2023.109260.
- [18] X. Zhang, Q. C. Zhong, W. L. Ming, "Stabilization of a cascaded DC converter system via adding a virtual adaptive parallel impedance to the input of the load converter", *IEEE Transactions on Power Electronics*, vol. 31, no. 3, pp. 1826–1832, 2016, doi:10.1109/TPEL.2015.2469720.
- [19] S. Augustine, M. K. Mishra, N. Lakshminarasamma, "Adaptive droop control strategy for load sharing and circulating current minimization in low-voltage standalone DC microgrid", *IEEE Transactions on Sustainable Energy*, vol. 6, no. 1, pp. 132–141, 2015, doi:10.1109/TSTE.2014.2360628.
- [20] Y. Mi, J. Guo, S. Yu, P. Cai, L. Ji, Y. Wang, D. Yue, Y. Fu, C. Jin, "A Power Sharing Strategy for Islanded DC Microgrid with Unmatched Line Impedance and Local Load", *Electric Power Systems Research*, vol. 192, no. June 2020, p. 106983, mar 2021, doi:10.1016/j.epsr.2020.106983.
- [21] B. C. Moura, P. J. dos Santos Neto, L. F. Resende Bonnas, J. P. Carvalho Silveira, G. B. de Lima, L. C. Gomes Freitas, "Adaptive Droop Control to Reduce Steady-State Power Imbalances in DC Microgrids", in *2023 IEEE 8th Southern Power Electronics Conference and 17th Brazilian Power Electronics Conference (SPEC/COBEP)*, pp. 1–8, IEEE, nov 2023, doi:10.1109/SPEC56436.2023.10408419.
- [22] T. Castillo-Calzadilla, M. A. Cuesta, C. Olivares-Rodriguez, A. M. Macarulla, J. Legarda, C. E. Borges, "Is it feasible a massive deployment of low voltage direct current microgrids renewable-based? A technical and social sight", *Renewable and Sustainable Energy Reviews*, vol. 161, no. January, p. 112198, 2022, doi:10.1016/j.rser.2022.112198.
- [23] T. Dragičević, X. Lu, J. C. Vasquez, J. M. Guerrero, "DC Microgrids - Part II: A Review of Power Architectures, Applications, and Standardization Issues", *IEEE Transactions on Power Electronics*, vol. 31, no. 5, pp. 3528–3549, 2016, doi:10.1109/TPEL.2015.2464277.
- [24] R. W. Erickson, D. Maksimović, *Fundamentals of Power Electronics*, Switzerland: Springer, 2020.
- [25] I. Barbi, *Modelagem de conversores CC-CC empregando modelo médio em espaço de estados*, Author's edition, 2014.
- [26] J. M. Guerrero, J. C. Vasquez, J. Matas, L. G. De Vicuña, M. Castilla, "Hierarchical control of droop-controlled AC and DC microgrids - A general approach toward standardization", *IEEE Transactions on Industrial Electronics*, vol. 58, no. 1, pp. 158–172, jan 2011, doi:10.1109/TIE.2010.2066534.
- [27] D. Chen, L. Xu, L. Yao, "DC Voltage Variation Based Autonomous Control of DC Microgrids", *IEEE Transactions on Power Delivery*, vol. 28, no. 2, pp. 637–648, apr 2013, doi:10.1109/TPWRD.2013.2241083.

## BIOGRAPHIES

**Beatriz Cristina Moura** received a B.Sc. and M.Sc. in Electrical Engineering from the Faculty of Electrical Engineering at the Federal University of Uberlândia. She is currently a Ph.D. student in the Faculty of Mechanical Engineering at the State University of Campinas.

**Pedro José dos Santos Neto** is a professor in the Faculty of Mechanical Engineering at the State University of Campinas. He holds a Ph.D. and an M.Sc. in Electrical Engineering from the State University of Campinas and received his B.Sc. in Electrical Engineering from the Federal University of the Vale do São Francisco.

**Danillo Borges Rodrigues** received a B.Sc., M.Sc., and Ph.D. in Electrical Engineering from the Federal University of Uberlândia (UFU). He is currently a professor at the Federal University of Triângulo Mineiro and conducting postdoctoral research at UFU.

**Érico Chagas Guimarães** received his B.Sc. (2013) and M.Sc. (2016) in Electrical Engineering from the Federal University of Uberlândia. He is currently a Ph.D. student in Electrical Engineering at the same institution.

**Luiz Carlos Gomes Freitas** received his B.Sc. in Electrical Engineering, as well as his M.Sc., and Ph.D. degrees in Electrical Engineering from the Federal University of Uberlândia in 2001, 2003, and 2006, respectively. In 2008, he joined UFU as a faculty member, in which he currently develops teaching and research activities in the areas of power electronics and power systems.

**João Pedro Carvalho Silveira** received his B.Sc. and M.Sc. in Electrical Engineering from the Faculty of Technology at the University of Brasília. He earned his Ph.D. in 2022 from the Faculty of Electrical and Computer Engineering at the State University of Campinas. Presently, he has been collaborating as a professor at this same institution, as well as conducting postdoctoral research.

**Gustavo Brito de Lima** received his B.Sc., M.Sc., and Ph.D. degrees in Electrical Engineering from the Federal University of Uberlândia (UFU) in 2010, 2012, and 2015, respectively. In 2017, he joined UFU as a faculty member, where he currently develops teaching and research activities in the area of power electronics.